Trials and in silico simulations to predict daily photo-oxidative capacity under solar conditions: A case study on the inactivation of an oyster pathogenic bacteria, Vibrio harveyi

Cécile Blanchon, Eve Toulza, Christophe Calvayrac, Christophe Stavrakakis, Stanislawa Eichendorff, Gael Plantard

Trials and *in silico* simulations to predict daily photo-oxidative capacity under solar conditions: A case study on the inactivation of an oyster pathogenic bacteria, *Vibrio harveyi*

Cécile Blanchon[1,2,3,4], Eve Toulza[1], Christophe Calvayrac[2,3], Christophe Stavrakakis[5], Stanislawa Eichendorff[4], Gael Plantard[4]

[1] IHPE, Univ Perpignan Via Domitia, CNRS, IFREMER, Univ Montpellier, Perpignan, France

[2] Biocapteurs Analyses Environnement, Université de Perpignan Via Domitia, 66000 Perpignan, France

[3] Laboratoire de Biodiversité et Biotechnologies Microbiennes (LBBM), Sorbonne Universités, CNRS, 66650 Banyuls sur Mer, France

[4] PROMES-CNRS UPR 8521, Process Material and Solar Energy, Rambla de la Thermodynamique, 66100 Perpignan, France

[5] Ifremer – EMMA Plateforme Expérimentale Mollusques Marins Atlantique, F85230 BOUIN France

Abstract

In today's world of increasing seafood demand, aquaculture is crucial for food security. High population densities in fish and mollusk farms often cause frequent disease outbreaks, leading

to antibiotic use and genetic selection. However, emerging pathogen strains and antibiotic-resistant bacteria necessitate new bio-secure disinfection processes for aquaculture water. Current systems rely on filtration and UVC treatments, but Advanced Oxidation Processes (AOPs) present a promising solution for eliminating contaminants in seawater. While abiotic decontamination via photocatalysis is well-studied, biotic disinfection, particularly in seawater, remains underexplored. Heterogeneous photocatalysis effectively removes microbial and chemical contaminants, such as toxins, from seawater. This study aimed to assess the capacity of a solar photo-oxidation reactor for aquaculture water treatment plants. We defined and tested an inactivation kinetic law representing bacterial concentration changes for the oyster pathogen *Vibrio harveyi*. A kinetic model with orders of 1.23 for *V. harveyi* and 0.23 for flux density was selected. Photo-oxidation capacities were simulated under various reactor operating conditions using solar irradiation data from three French aquaculture sites, accounting for meteorological and seasonal variations. To address flux density variations caused by cloud cover and daily cycles, the flow rate was adjusted to ensure constant pathogen concentration at the reactor outlet. Results show that UV/TiO_2 disinfection effectively inactivates *V.harveyi*-contaminated seawater, offering scalable, sustainable solutions for aquaculture biosecurity.

Keywords: *Vibrio harveyi*, solar photocatalysis, oyster pathogens, inactivation, disinfection, simulation.

1. Introduction

Oyster production represents a significant part of aquaculture, with a strong increase in demand. Since several years, this production has been subject to heavy losses due to recurrent

mortality episodes [1–6]. Most oyster mortalities are caused by bacterial and/or viral infections leading to the death of the animals. These pathogen infections can affect animals throughout their lives, sometimes decimating entire farm productions. Several production stages are carried out in closed land-based ponds with controlled water quality. Among the stages carried out in onshore facilities are larval development and growth, which take place in hatcheries. Similarly, juvenile and spat oysters can be grown on land in facilities known as nurseries. In these facilities, the oysters/larvae are placed in closed batch tanks or continuously supplied with seawater disinfected by filtration and UVC treatment, especially in hatcheries [7–10]. A number of systems for filtering water (membrane process, carbon column) have been developed on an industrial scale [11–16] mostly for the elimination of abiotic contaminant. To ensure pathogens elimination filtration need to be coupled to UVC treatment. However, these technologies are costly both in terms of construction, operation and energy demand [17].

Currently, few new technologies are being developed for the biosecurity of aquaculture ponds, whether in freshwater or seawater. To address cost and energy demand issues while allowing sufficient disinfection and decontamination level of the seawater all at once, advanced oxidation processes, and in particular photochemical processes, appear to be a promising alternative as only one process is needed and the solar energy can be used. These processes, based on the use of catalysts in soluble (photosensitive reagents) or solid (photocatalysts) form, enable radiation to be photo-converted into reactive chemical species [18–20]. It consists in a photo-excitation process in which the catalyst absorbs radiation to release charges (electron-hole pairs), which initiate oxidation-reduction reactions. These reactions lead to the production of chemically unstable radical species capable of breaking the carbon-carbon bonds of organic compounds. This photo-conversion process is widely studied

in the literature for the detoxification of abiotic contaminants (pharmaceuticals, biocides) [21–23] but also for water disinfection [24–27]. Most studies have been carried out on effluents and wastewater but work on disinfection in seawater is emerging especially about *Vibrio* inactivation [28–30].

In this context, the heterogeneous photocatalysis process is an alternative offering the possibility of exploiting the solar resource [31]. Like other solar processes, the performance of this technology is closely dependent on the availability of the resource [21,31,32]. It is characterized by discontinuities on several scales, linked to daily (day/night alternation) and seasonal cycles, which will define the amount of energy available [23,33]. The energy available therefore depends on the duration of daily sunshine and the level of radiation received [34,35]. Weather conditions (strong sunshine, cloudy periods) and location (latitude, annual sunshine) should also be taken into account when assessing photo-conversion capacity [21,23,36].

In order to design solar installations capable of ensuring the biosecurity of aquaculture waters, the performance of oxidative photoreactors must be established taking into account the specific characteristics of the solar resource and the targeted pathogen. To do this, two key points need to be considered in order to establish the capacities of the photoreactor operating in continuous mode under dynamic irradiation conditions. The first is to define a kinetic law representative of the photodegradation process of the bacterial target. In the literature, numerous laws have been proposed to describe the degradation of abiotic contaminants [21,37–39], which are mainly empirical laws or formalisms that take into account degradation phenomena and the mass transfer of targets to the surface of catalysts. Concerning disinfection, the number of laws is more limited. Since the inactivation process is not immediate, several successive radical attacks are required to damage the membrane of

bacterial targets [40–42]. Once the membrane is degraded, bacterial inactivation becomes effective, resulting in a sharp drop in the number of viable bacteria. To describe inactivation profiles in most conditions, empirical models based on a power law according to concentration, involving parameters of no physical or chemical significance, have been developed [25,42–49]. Langmuir-Hinshelwood type models, directly inspired by the laws used for the mineralization of organic pollutants, have also been proposed. These models include an initial lag time to account for the multiple radical attacks required to initiate inactivation, but do not consider the effect of irradiation level. More recently, authors have proposed to represent the inactivation rate as a function of two key variables: bacterial concentration and flux density [24–26,50–53].

A description of the functioning of a photoreactor operating in continuous mode requires its configuration to be taken into account, in terms of geometry (tubular, planar) [12,32,54], operating mode (batch or continuous) [22,23], and operating conditions applied, *i.e.* the concentration level, flux density and flow rate [55,56]. A process engineering approach, the mass balance, including a feed term and a kinetic term, is used to formalize the capacity of the photoreactor under dynamic irradiation conditions [12,23,38,57]. It is thus possible to predict the daily capacity of the photoreactor under irradiation conditions representative of different sunshine conditions.

The aim of this paper was to represent the capacities of the photoreactor operating under simulated solar irradiation conditions in order to being able to predict and scale up seawater treatment facilities intended for aquaculture. A formalism based on kinetic laws from the literature is proposed in order to select a kinetic law representative of the *V. harveyi* inactivation process and to identify the kinetic parameters. Based on the established law, the

capacities of the photoreactor operating under different irradiation conditions were determined to define the importance of sunshine conditions (period of year, day length, meteorological conditions) at three oyster farming sites. Based on the daily capacities obtained, this study proposes, on one hand, a solution for managing discontinuities in the solar resource on different scales (day/night cycle and cloudy periods) and, on the other hand, the scaling up of installations dedicated to the biosecurity of aquaculture water.

2. Materials & Methods

2.1. Photoreactor

Photo-oxidation experiments were conducted (Fig. 1) using TiO_2 microparticles from commercial TiO_2 powder VP Aeroperl with an average diameter of 41 µm. TiO_2 smallest particles were removed by multiple decantation to improve the downstream separation to have a standard deviation of the size distribution of 17 µm [33]. The catalyst concentration has been optimized in previous work to capture all the incident radiation. The optimal concentration of 4 $g.L^{-1}$ of TiO_2 found for freshwater decontamination using this photoreactor was applied for disinfecting seawater [56].

The pilot operated in batch mode. It is composed of three parts as is reported in Fig. 1 [24,57]. The photoreactor is composed of an agitated irradiated volume of 0.3 L (0.15 m x 0.1 m x 0.02 m). To ensure even distribution of the catalysts in the suspension, the photo-reactor is equipped with a magnetic stirrer and a pump-controlled recirculation loop. The irradiated face was in a 95% UV-transparent polymethyl methacrylate (PMMA). Irradiation was carried out using a panel made up of 16 LEDs, which ensured that the radiation was evenly distributed over the surface of the photoreactor. This system has been detailed

and validated in previous work [57]. The LEDs emit ultraviolet radiation with an emission spectrum centered around 375 nm (the emission spectrum is shown in supplementary 1). The applicable flux density is between 0 and 45 $W.m^{-2}$. The flux density can be adjusted via a software interface to an accuracy of ± 0.1 $W.m^{-2}$. This system can also be used to apply dynamic irradiation setpoints, such as the flux density representative of radiation over the course of a day's sunshine. The distribution of radiation on the surface of the photo-reactor was checked using a UV solar sensor (UV Radiation, apogee instruments). The variations in flux density over the surface are of the order of ± 1 $W.m^{-2}$. The last part of the pilot is the recirculating loop of 50 mL to assure a perfectly homogenized reactor. The fluid flow is driven by a centrifugal pump (Cole Parmer).

Before each disinfection experiment, the photoreactor was sterilized using 0.1 M of NaOH followed by milliQ water rining.

All the photo-oxidative experiments were conducted in triplicate.

2.2. Biological material

An oyster pathogen, *Vibrio harveyi Th15_O_G11* modified with a stable Green Fluorescent Protein (GFP) plasmid with trimethoprim resistance pFD086 (GFP, TrimR) [4] was used to study the disinfection process. *V. harveyi* cells (*Th15_O_G11 GFP*) were grown under sterile conditions in 200 mL of Zobell medium (4 $g.L^{-1}$ bactopeptone, 1 $g.L^{-1}$ yeast extract in sterile seawater, pH 7.4) with 10 $\mu g.mL^{-1}$ of trimethoprim (T7883, Sigma Aldrich, France) at 20 °C until the stationary phase was reached. The bacterial growth was monitored by optical density at 600 nm (UV-1800, Shimadzu, France). Cultures in the stationary phase were appropriately diluted in sterile natural seawater (Banyuls, France, pH 8 and salinity adjusted to 35 PSU) to reach the desired concentration at the beginning of the photo-oxidative

treatments. The Banyuls seawater was follow and analyzed by the SOLOMIT project and all the data are available online [58]. Before inoculation, some of the suspended particles were removed by 1 µm seawater filtration, followed by autoclave sterilization to ensure that only our target bacteria are present.

Disinfection was monitored by the enumeration of cultivable bacteria on agar plates with a detection limit of 10^2 CFU/mL. The culture medium was Marine Agar (Marine Broth medium with 15 $g.L^{-1}$ of agar, 76448, Sigma Aldrich, France) with 10 $\mu g.mL^{-1}$ of trimethoprim and all countings were performed in triplicate by drip deposit of 10 µl of a range of serial dilutions of treated seawater in Lewis seawater (supplementary 2) [59]. Then, agar plates were incubated at 20 °C for 24 h until counting. In addition to the trimethoprim screen, the fluorescence of the colonies was checked at 395 nm (Lepro Lampe Torche UV LED) before cultivable bacteria enumeration to check for potential contaminants. For all counts, a 200 µl spread of sterile seawater (prior to bacterial inoculation) was used as a negative control to check for the presence of contaminants in the seawater prior to inoculation.

3. Photocatalysis kinetic law

To determine the disinfection capacity of a photoreactor, we described the phenomenon both at the scale of the inactivation reaction and at the level of the complete reactor [25,36,57]. At the reaction level, we need to express a kinetic law representative of the photo-oxidation process taking place in the photoreactor. This process must represent both the limits of radical production and the degradation of the target. At reactor level, the aim was to formalize the variations in the quantity of matter occurring during the treatment, which are formalized by a mass balance. This balance takes into account the reactor configuration, its operating mode and the operating conditions applied.

3.1. Kinetic law formalism

Bacterial disinfection follows a 3-step process. In the initial stages of the treatment, the bacteria experience damage. However, multiple instances of damage are necessary to hinder the growth process, as previously highlighted in several studies [60–63]. This requirement for multiple damage events results in an initial shoulder in the disinfection kinetics. As the treatment progresses, the cumulative damage inflicted on the bacteria eventually leads to their inactivation. This degradation process can be accurately represented by the photocatalysis kinetics law. After several hours of treatment, a phase characterized by a stabilization in bacterial concentration, often referred to as tailing off, becomes apparent. This phenomenon can be attributed to various factors. It might be associated with the emergence of bacterial strains that have developed resistance to the treatment, or it could be due to limitations such as the detection threshold of the culture method or mass transfer constraints [60–63].

In addition, the inactivation profile depends on the specific bacteria-catalyst combination. This variability adds complexity to the task of formulating a universally applicable process suitable for all target microorganisms making impossible the establishment of a universal kinetic law. To date, many formalisms have been developed for bacterial inactivation by photocatalysis in freshwater, but none of them has achieved consensus [25,42–49]. Nevertheless, the majority of the expressions are based on the dependence of the inactivation rate on the target concentration [29,42–47,49,64,65]. Only few kinetic laws translate at the same time the impact of both the target concentration and the flux density applied [24,25]. However, the impact of flux density is a key parameter to describe the capacity of the photoreactor particularly for solar applications. In this context and considering

that the incident photons are not applied on the closed fluid loop but only on the irradiated reactor volume V_r (L) across the irradiated surface *S,* the generic formalism, eq. (1), was written to consider both impact of incident photon quantity and bacterial quantity.

$$\dot{r} = \alpha.\frac{(S.I_{(t)})^f}{\beta.S.I_{(t)}+1}.\frac{(V_r.C)^n}{\beta'.C.V_r+1} \qquad (1)$$

with *S* the irradiated surface of the reactor (m^2), V_r the irradiated reactor volume (L), *I* the flux density directly measured as a function of the exposition time ($W.m^{-2}$), and *C* the *Vibrio harveyi* concentration at the time t ($cfu.L^{-1}$). The photo-conversion efficiency was carried out by the constant α ($s^{f-1}.J^{-f}.cfu^{1-n}$).

In this kinetic law, the β' and n constants reflect the inactivation rate limitation by mass transfer. The adsorption/desorption equilibrium between bacteria and the surface of the photocatalyst is reflected by the Langmuir constant β' (cfu^{-1}). The photons absorption / Reactive Oxygen Species (ROS) production equilibrium is reflected by the Langmuir type constant β (W^{-1}) and the f constant. For example, a value of f equal to 1 and β to 0 translates a linear dependence of the inactivation rate to the incident photon quantity, meaning that photon absorption is linearly related to the flux density applied. In this case there is no limitation by catalyst due to photon absorption. The ROS production rate is directly related to the flux density. Similarly, a value of f superior to 1 reflects a saturation of the catalyst by incident photons leading to a decrease of the photo-conversion efficiency.

The specific case of pseudo first-order kinetic law described in the literature can be represented by the following constant value, n equal to 1, with β and β' are equal to 0. This representation shows the direct and proportional dependence of the inactivation rate to the target concentration and to the flux density [25].

In this context, and as the identification of the law was done empirically it is preferable to have limited number of parameters so, five formulations of the rate of bacterial inactivation derivated from the rate of inactivation present in eq. (1) were selected (eq. (2) to (6)). Those formulation were chosen to always consider both the effect of the flux density and the target concentration on the target inactivation.

$$\dot{r} = \alpha.(S.I_{(t)})^{f}.C.V_r \quad (2)\ \text{Model N°1}$$

$$\dot{r} = \alpha.(S.I_{(t)})^{f}.\frac{C.V_r}{\beta'.C.V_r+1} \quad (3)\ \text{Model N°2}$$

$$\dot{r} = \alpha.(S.I_{(t)})^{f}.(C.V_r)^{n} \quad (4)\ \text{Model N°3}$$

$$\dot{r} = \alpha.(C.V_r)^{n}.\frac{S.I_{(t)}}{\beta.S.I_{(t)}+1} \quad (5)\ \text{Model N°4}$$

$$\dot{r} = \alpha.\frac{S.I_{(t)}}{\beta.S.I_{(t)}+1}.\frac{C.V_r}{\beta'.C.V_r+1} \quad (6)\ \text{Model N°4}$$

3.2. Mass balance formalism

Several authors have already reported that the inactivation of bacteria by photocatalysis in freshwater encompasses several concurrent mechanisms [25,26], with the primary ones being photolysis and photocatalysis. Photolysis directly results in bacterial inactivation through the direct effects of radiation, playing a significant role in degrading bacteria in solution. In contrast, photocatalysis is a more intricate process involving various steps. Firstly, as degradation can only occur in the immediate vicinity of the catalyst, mass transfer (both target and photon) plays a key role. This encompasses the migration of bacteria from the liquid phase to the solid catalyst surface, along with the transfer of photons to the catalyst. Once species are in proximity to the catalyst, photon absorption and bacterial adhesion occurs. Photon absorption initiates the generation of radicals (ROS) responsible for bacteria degradation. Lastly, the desorption of degraded bacteria is also crucial, allowing for the

release of catalyst active sites for the adhesion of other intact bacteria. Hence, Kacem et al. have highlighted the importance of writing mass balances considering both mass transfer in the reactor (photon and bacterial transfer) and disinfection kinetics [24,25]. To this end, terms for catalyst adhesion and inactivation kinetics have been written. As some of the incident photons may react directly with organic species present in the medium, a photolysis inactivation term can also be added. But none of those models have been developed for seawater inactivation. The objective is to determine the kinetic law of *V. harveyi* inactivation in natural seawater.

We conducted preliminary experiments at high flux density at 45 $W.m^{-2}$ to assess the photolysis of *Vibrio harveyi*. At this flux density, photolysis-induced inactivation remained below 20% even after prolonged irradiation, exhibiting a significantly lower inactivation rate compared to photocatalysis. Therefore, we decided not to model the contribution of photolysis-induced degradation since it was considered negligible.

Similarly, we have previously conducted adhesion experiments and found that, under the specific experimental conditions, mass transfer was not a limiting factor [66]. Furthermore, as adhesion was not a limiting factor, its impact on photocatalysis was also excluded from consideration.

In addition as bacteria can be sensitive to temperature we ensure the temperature inside the photoreactor did not exceed 5°C variation throughout the photocatalysis treatment.

Series of photocatalytic experiments were performed in triplicate with an incident flux density ranging from 10 to 45 $W.m^{-2}$. For all the *Vibrio* initial concentration (ranging from 10^4 to 6.10^5 $cfu.mL^{-1}$), the inactivation at the end of photocatalysis experiment was more than 99% (more than 2 log inactivation). As it was already reported, the bacterial death do not occur immediately at the start of the treatment, as many ROS attacks are needed to inactivate

a bacteria leading to a shoulder at the beginning of the photocatalytic treatment [60–63] so we developed a two-step model, eq. (7). As no adhesion or photolysis were observed with the strain of *Vibrio harveyi* used, the mass balance of the reactor can be summarized in batch to the kinetic law. This equation was written to represent the variation of the bacterial quantity inside the reactor.

As presented before, the pilot was composed of an irradiated reactor where the photocatalytic reaction takes place and a recirculation loop to guarantee a perfectly mixed reactor. The mass balance applied to the target bacteria (*C*) in the process yield the following expression considering the overall system reactor as a perfectly mixed reactor (concentration gradient inside the reactor was very small):

$$\begin{cases} \frac{V_T.dC}{dt} = 0, & for\ t < t_{shoulder} \\ \frac{V_T.dC}{dt} = -\dot{r}, & for\ t > t_{shoulder} \end{cases} \quad (7)$$

This mass balance uses a conditional statement, a common practice in the literature, to characterize the initial shoulder phase. As a result, two balance equations are formulated: the first describes the shoulder phase, in which the population of viable bacteria remains constant despite ROS attacks, and the second portrays photocatalytic inactivation in line with the kinetic law. In those equations, $V_T = V_r + V_{loop}$ is the total volume of the reactor (L) comprising the irradiated volume and the volume of fluid in the recirculated loop, and $\dot{r}$ is the kinetic law of the bacterial inactivation rate (eq. (2) to (6)).

The reactor can be used in two different ways, the first was the batch mode that we have present previously, and the second was the continuous mode or open mode. In this mode, the photoreactor was constantly supplied with the seawater containing the bacteria meaning that new contaminant (bacteria) was constantly adding to the reactor (the feeding). In the

meantime, a part of the liquid was removed from the reactor to ensure that the reactor volume remain the same (the withdrawal). For continuous operating of the reactor, this balance needs to take into account the continuous feed of bacteria (first term of eq. (8)), its degradation in the irradiated photoreactor (third terms of eq. (8)) and the withdrawal of part of the seawater treated with the photoreactor presented above (second term of eq. (8)). Moreover, the mass balance with conditional statement as present in eq. (7) was no longer used as a transitory phase perfectly describe by the eq. (8) was observed instead of the shoulder.

$$\frac{V_T.dC}{dt} = q.C_0 - q.C - \alpha.(S.I_{(t)})^f.(C.V_r)^n \qquad (8)$$

with q the flow rate for the feed and racking of the reactor ($L.s^{-1}$) and C_0 the target bacteria concentration in the photoreactor feed solution ($cfu.L^{-1}$). Given the thorough agitation in the photoreactor, the target bacteria concentration remains uniform throughout the reactor. Consequently, the bacterial concentration at the reactor outlet accurately mirrors the concentration within the reactor.

3.3. Solar irradiation characteristics

To assess the photo-oxidative capacities of a photoreactor under natural solar irradiation, dynamic conditions found in several oyster farming regions in France were applied. This approach consists in applying irradiation set-up representative of varying solar resource characteristics, such as daily cycles and seasonal variations such as day length, incident solar flux, and the influence of weather patterns. For this study, we selected three cities situated near oyster farms along the French coastline: Bordeaux and Nantes on the Atlantic coast and Montpellier (Thau lagoon) on the Mediterranean coast. Simulations were conducted with a photoreactor operating under open mode. The kinetic law (Eq. 4) number 3 was used with the

corresponding parameters identified (Table 1). The mass balance presented in Eq. 8 was employed to describe the performance of a photoreactor continuously supplied with a solution containing *Vibrio harveyi*. The photoreactor was subjected to dynamic irradiation profiles that represent weather conditions in the selected cities.

The solar resource fluctuates around periods and places, and is by nature a discontinuous resource at several scales. It is highly dependent on location, but also on the period of the year. In fact, in addition to fluctuating with the alternating day/night cycle, solar resources also depend on the cycle of the seasons [32,34,35,67,68].

Resource availability depends significantly on the length of the day and the flux density received. Depending on the period of year, the day duration will change (Table 2), the shorter day is the winter solstice (December 21st) and the longer is the summer solstice (June 21st). Days are almost twice as long in summer as in winter (15h in July *vs.* 8h in January). Moreover, the flux density received also changes with the season (Fig. 5a) leading to an increase of the cumulative energy received on an average day in summer (July) of more than 75% compared to winter (December) (Table 2). For example, the maximum flux density can reach 50 W.m^{-2} in July, compared with 25 W.m^{-2} in December.

Resource availability fluctuates even on shorter time scales, particularly during daily periods of cloudiness. These transient cloud cover events have a substantial influence on resource availability by strongly altering the incident flux density. For instance, as depicted in Fig. 5b, a cloudy day in July leads to a two-fold reduction in cumulative flux density when compared to a clear, sunny day. Geographical location plays an essential role in this context. The three sites chosen to represent French oyster-growing areas located in regions with distinct climatic conditions. In winter, the difference between sites is greater than in summer, with 21% more cumulative energy received between Bordeaux and Nantes in January,

compared with just 5% in July. In addition to variations between months, there are also variations within a month on the same site (Fig. 2a and b). For example, in July in Montpellier (southern France, along the Mediterranean Sea), the flux density received can vary from 10-20 $W.m^{-2}$ on cloudy days to over 45 $W.m^{-2}$ on sunny days (Fig. 5b).

Taking into account the spatio-temporal characteristics of solar resources is essential for assessing photoreactor performance. This approach enables photoreactor capacities to be used to predict daily and monthly processing capacities. These considerations are crucial to adapting the system size to the location and period of operation.

Moreover, it is crucial to note that the solar resource is composed of a large range of UV (UVA, UVB and UVC) compared to laboratory lamp that have limited range of UV leading to potential variation on the bacterial inactivation. UVC and UVB are much more energetic inducing much more damages to cells than UVA but also more less abundant. For example, Schuch et al. present UV absorption by DNA and the oxidative damage done to it in their revue and discuss the fact that UVA can do many damages due to it high abundance (more than 20-fold UVA than UVB on Earth's surface for only 4.2-fold less absorption by DNA) [69]. Here bacterial inactivation by solar irradiation were predict based on work done only with UVA light at lab scale by it was assume that inactivation tendance will remain the same using solar light assuming than it is mainly composed of UVA. However, as UVB (and few UVC) are also present in the solar spectra, the intensity of the inactivation will be increased under real solar irradiation compared to UV lamp leading to a more efficient inactivation.

4. Results

4.1. Batch photocatalytic reactor, determination of the kinetic law.

The aim of this section was to determine the appropriate kinetic law and to identify the kinetic parameters. The selected laws allow good fitting of the *Vibrio harveyi* inactivation on natural seawater (containing a multitude of salt and other organic residues) while limiting the number of undetermined parameters to a maximum of 3. This allowed us to obtain a simple kinetic law highlighting the limitations of both the quantity of incident photons and the quantity of bacteria. The identification of the unknown parameters (α, β, β', n, and f) was performed in Matlab software using the Nelder-Mead simplex algorithm [70] by minimizing the mean relative error (MRE) define in eq. (9). This criterion compares the calculated concentration profiles obtained using the *ode45* solver to the experimental results. The unknown parameters were optimized using an experimental dataset of 15 independent experiments with four UV irradiation levels ranging from 10 to 45 $W.m^{-2}$ and target initial concentration ranging from 10^4 to 5.10^5 $cfu.mL^{-1}$.

$$MRE = \frac{1}{n_{exp}} * \sum_{i=1}^{n_{exp}} \left| \frac{C_{exp\_i} - C_{simulation\_i}}{C_{exp\_i}} \right| * 100 \qquad (9)$$

with n_{exp} the number of experiments used for the optimization, C_{exp} and $C_{simulation}$ the dataset from the experience and from the simulation respectively.

As shown in Fig. 2, the average kinetics of the experimental data used to identify the laws all show a shoulder followed by a decrease in bacterial concentration. This profile is in accordance with the literature [60–63]. The fitting of these experimental curves with all the kinetic laws allows an MRE lower than 10% (Table 1).

The kinetic law defined by equations (4) was the best to describe our experimental inactivation curves with the lowest MRE (Table 1). This law describes the inactivation limitation by high flux density which is leading to a slowdown in the inactivation rate. When the flux density is too high, the received photons are too important, the catalyst cannot generate all the ROS corresponding, resulting in a decrease of the photo-conversion efficiency in accordance with the dependency lower than one on the flux density I. The Fig. 3 shows the fitting of the average experimental curve for each condition with the best kinetic curve found. In this kinetic law, the f value was found to be of a similar order of magnitude (around 0.3) as the values typically reported in the literature for abiotic targets in freshwater (typically around 0.7) [54]. The f value was lower than 1, reflecting a limitation in photon transfer in the medium. One hypothesis for the higher limitation in seawater compared to freshwater would be the absorption of part of the incident photons by salts and other suspended matter.

To validate the selected kinetic law (Eq. 4), two additional batch experiments at 45 $W.m^{-2}$ and around $5x10^4$ $cfu.mL^{-1}$ were performed. Fig. 4 shows the comparison between experimental results and *in silico* inactivation profiles calculated with the kinetic law found previously and the linear kinetic law. The applied kinetic law and mass balance allowed a good representation of parts of the experimental inactivation curve. The relative error between experimental inactivation and simulated inactivation curves was lower than 15% (Fig. 4a and b). Considering standard deviations on experimental measurements (Fig. 4c), the kinetic law N°3 (eq. (4)) was used for the following part. It was a simple law with only three constants that also allows us to well represent our experimentations by considering both the effects of flux density and bacterial concentration on the inactivation rate.

4.2. Photo-oxidative capacity simulation under daily conditions in continuous flow: influences of sunshine discontinuities.

To assess the photo-oxidative capacities of the photoreactor under natural solar irradiation, the dynamic conditions found in several oyster farming regions in France were applied. We investigated the reactor's operation under various feeding conditions, including a range of feed concentrations resembling those found in nature, as well as different photoreactor flow rates, resulting in distinct residence times within the photoreactor.

4.2.1. Impact of operating conditions on inactivation rate

Based on the mass balance of the photoreactor operating in open mode (eq. (8)), inactivation kinetics have been simulated under various operational conditions, such as flux density, bacterial concentration, and flow rate. Fig. 6 illustrates examples of the curves generated for specific fixed operational parameters throughout the inactivation processus. Under all operational scenarios, the inactivation curve can be divided into two distinct phases. The first phase represents the transient step, where the bacterial concentration in the reactor decreases until reaching an equilibrium state. The duration of this transient mode is directly related to the hydraulic time (residence time of bacteria in the reactor) and to the operating conditions. For example, a change in flux density or flow rate will lead to a disturbance in the system, resulting in transient functioning. When the photoreactor is operating under solar irradiation, due to the discontinuity of the flux density applied the reactor is constantly in transient mode. In a second step, the reactor reaches a steady-state condition, in which, accumulation within the reactor is zero, *i.e*. there is no longer any variation in the quantity of bacteria. The quantity of bacteria introduced through the feed reaches an equilibrium with

the amount removed from the reactor, considering both degradation through photo-oxidation and removal through racking.

Examining the influence of each operating parameter individually, both the flow rate and flux density affect the duration of the transient phase and the achieved inactivation rate (Fig. 6a and c). Higher flux density leads to a faster attainment of the steady state with lower bacterial concentration in the reactor. Similarly, reducing the flow rate enhances bacterial inactivation. Lowering the flow rate increases the residence time in the reactor, thereby boosting bacterial inactivation. On the other hand, when the flow rate is too high, the bacterial input is too high compared to the inactivation and so the concentration at the reactor outlet is close to the one applied at the inlet. Conversely, while increasing the bacteria concentration of the feed affects inactivation kinetics, its impact is less pronounced (Fig. 6b).

Now, let's take a closer look at the influence of two key factors already established in the literature: flux density and feed concentration and their impact once reactor equilibrium is reached. Fig. 7a and b represent the inactivation rate once the reactor is in steady state as a function of the flux density (a) and the bacterial concentration (b).

In the literature, the reactor performances are correlated to the flux density, as it was showed for abiotic pollutant the quantum yield of the reaction is higher at low flux density and then decreases with the increasing flux density [71]. As shown in Fig. 7a, the rate of bacteria inactivation is strongly influenced by flux density by the amount of photons received. The influence of flux density on bacterial inactivation rate can be divided down into several parts. This pattern was already observed for abiotic pollutant such as phenol [37]. The inactivation rate is strongly dependent of the flux density below 25 $W.m^{-2}$. Then for flux densities superior to 25 $W.m^{-2}$, the inactivation rate slows down and tend to a plateau until

after 50 $W.m^{-2}$ no improvement is observed. The plateau observed for high flux densities reflects that the ROS production is maximal, enabling maximum target degradation [31,54].

Fig. 7b shows the variation of the inactivation rate as a function of the pathogen concentration in the feed solution. At low bacterial concentration, the inactivation rate was limited by the mass transfer. The mass transfer governs the photo-oxidation reaction, highlighting that bacteria must be in the vicinity of the catalyst particles for inactivation. Then, when the bacterial concentration is high enough, the rate of inactivation is correlated with the increase in bacterial concentration. Thus, the photo-oxidation reaction is governed by the reaction regime. For the three flux densities presented, the curves showing the evolution of the inactivation rate as a function of the reactor feed concentration overlap.

4.2.2. Solar irradiation influence

To evaluate the influence of sunshine conditions on the photoreactor's daily treatment capacity, treatment capacities were simulated for three oyster production sites and for each month of the year (average day, sunny day and cloudy day). Simulations were performed with irradiation data from Meteonorm software for three French cities (Bordeaux, Nantes and Montpellier). The simulations of bacteria inactivation for average monthly days in Montpellier (Fig. 8a), Bordeaux (Fig. 8b) and Nantes (Fig. 8c) were reported in Fig. 8 for a feed solution of 1 $mL.min^{-1}$ at 10^4 $cfu.mL^{-1}$ in a 0.3 L photoreactor (with an irradiated surface of 0.015 m^2).

On an average day, the inactivation kinetics consistently exhibit a common pattern, regardless of the city or period of the year. Three distinct phases are observed. During the morning, when irradiation levels are low, bacterial concentrations decline rapidly, reaching a plateau around mid-day. As the Fig. 7a show, the inactivation rate stabilizes at flux densities above 25 $W.m^{-2}$. However, at mid-day, whatever the location or season, flux density values

exceed this value. Consequently, the concentration in the photoreactor reaches a plateau when the flux density exceeds 25 $W.m^{-2}$. As the day progresses and the flux density decreases to zero in the evening, the bacterial concentration gradually rises, returning to the inlet concentration level. This profile fit with the literature for daily freshwater decontamination both for real and simulated irradiation [57].

A more detailed examination of monthly inactivation patterns reveals a consistent profile across different locations. In Montpellier, for instance (Fig. 7a), bacterial inactivation rates intensify in correlation with the amount of sunshine. High flux density months occurring during day length exceeding 13 h of irradiation (mostly summer months) have a higher inactivation levels compared to Winter months. Months with sunnier and longer days, such as Summer, exhibit higher inactivation rates as well as more prolonged maximum inactivation plateaus. Conversely, winter months, characterized by limited sunshine and shorter days, display lower inactivation rates and shorter plateaus. Transitional months with moderate sunshine, like spring and autumn, fall in between these two categories. When comparing winter and summer months, the duration of the maximum inactivation plateau is directly tied to the length of daylight. The day length, preferably before the level of flow density, is the key factor to determined photoreactor's capacity. It will impact the duration of photocatalysis and therefore the photoreactor's capacity by improving both the treatable volume and the total quantity of inactivated bacteria per day. On the other hand, the higher flux density (received during the summer months) enables us to achieve better inactivation rates (lower bacterial concentration). As observed in Fig. 7, the inactivation rate tends to a maximum at high flux densities, which explains the plateau in bacterial concentration during the mid-day. The same observation was done for other locations.

The comparison of the reactor's degradation capacity over the seasons shows that this is not significantly different. Moreover, the maximum inactivation rate in winter is only 0.2 logarithms lower than that in Summer, attributed to the inactivation rate's dependence on flux density, which follows a 0.23 order pattern. The degradation capacity of the reactor is strongly correlated to the irradiance. As depicted in Fig. 7, once irradiance exceeds 25 $W.m^{-2}$, the inactivation rate experiences minimal variation, resulting in similar inactivation rates between winter and summer. The limitation by the flux density is particularly striking on Fig. 8d which represents the inactivation of *Vibrio harveyi* for all three locations in July. The flux density received by the photoreactor is different between the tested location, but the inactivation rate is similar. At Montpellier, during the day, the photoreactor receive more than 450 kJ with a maximum of 40 $W.m^{-2}$ versus around 375 kJ at Bordeaux and Nantes with a maximum of 35 $W.m^{-2}$. Those irradiations allow to achieve an inactivation of 2.5 log corresponding to an inactivation of 99.7% of the incoming bacteria. The same observation has also been done for all months.

Focusing now on the effects of weather conditions, irradiation between days varies significantly (Fig. 5). Looking at inactivation on three typical summer days in Montpellier (Fig. 8e), corresponding to a very sunny day (day 1 on Fig. 5b), a very cloudy day (day 2 on Fig. 5b) and an average day (day 3 on Fig. 5b). The influence of irradiation intermittencies on the photocatalysis efficiency is clearly visible. As Fig. 8e shown, on a cloudy day, the outlet concentration changes over the day according to irradiation (cloud passage). The average inactivation rate is $4.1x10^{3}$ $cfu.h^{-1}$ for a cloudy day of July in Montpellier versus $4.3x10^{3}$ $cfu.h^{-1}$ for a sunny day. The cumulative amount of energy received on a sunny day is twice more

than for a cloudy day with rapid and important variations of the flux density resulting on diminution of cumulative amount of energy received.

To conclude, the bacterial inactivation is driven by the total cumulative amount of energy received. This amount of energy is correlated to the level of irradiation and the sunshine duration. As the inactivation rate is stable for irradiation greater than 25 $W.m^{-2}$ the bacterial inactivation is primarily driven by the duration of daily irradiation, rather than the total irradiation received. Notably, as the bacterial inactivation rates are significantly influenced by irradiation fluctuations when irradiance remains below 25 $W.m^{-2}$ it still remains a relevant factor for low irradiance conditions such as during cloudy days when irradiance rapidly drops. However, across the multiple locations examined, this threshold value is typically surpassed. It is only during cloudy days that variations in irradiance have a notable impact on the inactivation rate and, consequently, on inactivation capacity. Therefore, to develop a real-time solution to effectively manage these intermittent conditions is crucial.

5. Discussion

5.1. How to manage solar intermittencies ?

Managing fluctuations in solar resources is one of the main challenges facing solar photocatalysis. To compensate for the fluctuation in solar resources, most authors focused on the development of new materials [72,73]. These materials, typically relying on activated carbons, offer the capability to store targets when sunshine is limited. Subsequently, during periods of intense sunshine, the targets present in the water can be effectively eliminated through photocatalysis. In the present work, the goal is to introduce an intermittence management system at the photoreactor scale by adjusting operational parameters, such as

the flow rate. The objective is to modulate the reactor's flow rate with prevailing sunshine conditions.

In a perspective of application for living organisms such as oysters, it is necessary to be able to guarantee a constant inactivation rate and seawater quality. We considered that treated seawater is sufficiently disinfected for aquaculture if the outlet bacterial concentration is less than 10 cfu.mL^{-1} with an input bacterial concentration of 10^3 cfu.mL^{-1} [74]. This corresponds to a bacterial inactivation of 99% (2-log inactivation). In the example of a photoreactor of 0.3 L (with an irradiated surface of 0.015 m^2) fed with a constant flow of 1 mL.min^{-1} of a solution at 10^3 cfu.mL^{-1}, this configuration will achieve less than 1.7 log inactivation (i.e. an inactivation of 98% of the incoming bacteria) at best of the day in July (Fig. 9). But, during cloudy days, the inactivation rate barely surpasses 96%. The treatable volume of seawater with 99% inactivation of the incoming bacteria was 0. So, this operation produces 9 L of seawater per week with an inactivation of 90% of incoming bacteria.

To achieve higher inactivation rates, modulate the retention time inside of the reactor by adapting the flow rate to the irradiations can be an alternative solution to increase the daily treatment volume while ensuring consistent quality at the reactor outlet (Fig. 9b) and maintaining a constant bacteria concentration regardless of irradiation, weather conditions, or day length (Fig. 9a). In this simulation, the constraint was to achieve and maintain an inactivation of 2 logs in the reactor, whatever the irradiation by adjusting the flow rate. For instance, on sunny days, such as the first day of the week in Fig. 9, it is possible to produce 200 mL with a *Vibrio* concentration lower than 10^2 cfu.mL^{-1}, whereas, on cloudy days (as indicated in Table 3) only 152 mL can be produced. While the treatable volume is somewhat reduced during cloudy days, the seawater quality at the photoreactor outlet is maintained during periods of low light irradiation, which includes cloudy periods, sunrise, and sunset. The

adjustable flow rate allows for the adaptation of the inactivation rate to weather conditions, thus mitigating its impact.

By adjusting the flow rate with irradiation conditions throughout the day, a consistent bacterial inactivation rate of 99% can be sustained from dawn to dusk. This results in a total volume of 1.3 liters of seawater disinfected at a 99% rate over the course of a week, in comparison to 0 liters disinfected to 99% when a constant flow rate of 1 $mL.min^{-1}$ is used. Employing a variable flow rate enhances the reactor's performance in terms of daily treatable volume and outlet seawater quality. However, it is important to note that as the flow rate is significantly reduced to enhance seawater quality, the average inactivation rate is likewise reduced (refer to Table 2 for the average inactivation rate). Therefore, by adjusting the photoreactor flow rate between 1 and 19 $mL.h^{-1}$ during the day, the bacterial concentration at the photoreactor outlet can be consistently maintained at over 90% of inactivation for one week (7 days). Modulating the flow rate enables reaching a more effective inactivation rate, even though it may limit the volume that can be treated. Conversely, maintaining a constant higher flow rate increases the treated water volume but does not ensure an adequate level of disinfection.

5.2. Photoreactor design for aquaculture facilities

This approach can be adapted to a solar installation that meets the demands of aquaculture facilities. The tools developed previously were applied to forecast the performance of a full-scale pilot system. This scale up was grounded in the kinetic law (eq. 4) and mass balance (eq. 8) established to determine the inactivation of *Vibrio harveyi* within a continuously operating photoreactor under solar irradiation. A solar photoreactor with a surface area of one square meter and a volume of 19.7 liters served as a reference to project

the treatment capacity of a facility. The predictions were generated with the goal of achieving a 99% reduction rate by adjusting the flow rate based on the irradiation levels. For each average day representative of the different months of the year in site (based on average day, Table 2), the retention time is adapted to the irradiation. It is therefore a matter of adjusting the flow rate to ensure 99% inactivation of the incoming bacteria. In these conditions, the treatable volume per day was reported in Table 4. For all three locations, the maximum treatable volume with suitable seawater quality is achieved in summer with 85L disinfected by day. In winter, due to less favorable irradiation conditions (both in terms of duration and quantity), the volume of seawater that can be treated is significantly lower, at around 30-40 L, a half the volume of sunny summer days.

In land-based aquaculture facilities like nurseries, the demand for water is substantial, often in the order of several cubic meters per hour per nursery tank [7,10]. Typically, oyster nurseries are generally made up of several large basins, each receiving a continuous supply of seawater. These basins serve for pre-growth of the oyster spats until they reach a weight of approximately 20 grams [75]. Due to this very large seawater demand, seawater is actually rarely disinfected in nurseries. For instance, considering a single nursery tank with a flow rate of 2 $m^3.h^{-1}$ in January, an 1 285 m^2 photoreactor with a volume of 25.3 m^3 would be required for Montpellier and a 1 543 m^2 photoreactor with a volume of 30.4 m^3 would be required for Nantes. If this is extrapolated to a real installation with multiple parallel tanks, the reactor size would need to be scaled up depending on the number of nursery basins, rendering the required reactor sizes impractical for such installations (more than a thousand square meters required for the photoreactor).

On the other hand, there are other aquaculture installations whose seawater requirements are lower in terms of quantity, that make them better suited to solar treatment.

For example, during the growth stages of oyster larvae, much less seawater is needed. The larvae are placed in batch tanks of a few cubic meters. The seawater in these tanks is occasionally renewed. Considering a hatchery with 3 m^3 tanks and based on the lowest treatable volumes (obtained with December irradiation, Table 4), a 86 m^2 photoreactor with a volume of 1.7 m^3 would be required for Montpellier and Bordeaux, and a 92 m^2 photoreactor with a volume of 1.8 m^3 for Nantes. Such photoreactors would enable seawater to be disinfected to a sufficiently high quality over a day. Hence, it becomes necessary to adjust the filling schedule of hatchery tanks in accordance with the availability of solar resources, such as using treated water during daylight hours to fill the hatchery tanks with disinfected seawater in the evening. Hatcheries do not have just one tank, but several parallel ones that also need to be filled. To optimize the use of the photoreactor for seawater disinfection and decontamination, it would be possible to fill the different tanks on different days. In addition, many facilities have seawater reserves of several hundred cubic meters upstream of nurseries and hatcheries. These seawater reserves are often subjected to natural solar irradiation with a large irradiated surface area and low seawater thickness, making them an ideal candidate for photocatalysis. These basins could be easily adapted for pool-type photoreactors which are proving to be robust and easy to use pilots [76].

The process as presented in this study with these treatment capacities and dimensions can also be adapted for experimental plants. In fact, these plants are scale models of industrial aquaculture plants and therefore require lower treatment volumes [8]. For example, Ifremer's marine mollusk platform (near Nantes, in Bouin, France) has a small hatchery for studying larval rearing, either continuously in small 5 L reactors or batchwise in 30 L tanks [8]. Considering the treatment capacities per square meter demonstrated in our study, it appears highly suitable to explore applications for this type of experimental facility. Like many

aquaculture facilities, the experimental platform features settling tanks of several hundred square meters in size, with low water volumes and large irradiated surfaces, facilitating the use of solar resources for photocatalysis [9]. In the case of experimental platforms, the effluent leaving the platform also needs to be disinfected before being released into the environment, to avoid discharging pathogens or other non-endemic biological compounds.

6. Conclusion

This study focused on the production of biosecure seawater for oyster farming and production applications using photocatalytic process. The water used must comply with certain constraints in terms of both biological quality and volumes available per day. In this context, a preliminary study aimed at estimating the daily capacity of a solar photo reactor was proposed based on biotic degradation using a three-stage approach.

The first part was dedicated to the selection of a kinetic model representative of the bacterial inactivation process, followed by the identification of the key kinetic parameters. A kinetic model, established with a number of reduced parameters, has proven to be representative of the experimental results obtained under different operating conditions. The experiments carried out for different concentrations of target bacteria and under different irradiation conditions were well represented by the selected model. This model also highlighted the influence of the two key variables, bacterial concentration and flux density.

The focus was then placed on predicting processing capacity under solar irradiation conditions. Irradiation setpoints representative of daily and monthly sunshine were applied. Fluctuations in irradiation conditions on a seasonal scale (length of day and daily flux density cycle), as well as intermittency linked to meteorological conditions, were taken into account to establish the photoreactor's capacity to treat the bacteria contained in seawater. First of

all, it emerged that the length of the day, which varies according to the season, is a key point for scaling up the reactor. Optimum daily treatment rates were achieved at low flux densities, and a concentration plateau, independent of high flux density, was obtained from the first few hours of sunshine. It has also been shown that the flux densities are insufficient to achieve a 99% inactivation rate, whereas the treatment is very effective in the middle of the day (higher than 99.99%).

In order to manage the intermittency of the solar resource, it was proposed to modulate the flow rate according to the irradiation conditions. The flow rate for each flux density received during the day has been adapted to comply with an inactivation rate of 99%. This alternative makes it possible to manage the intermittency associated with the solar resource, by obtaining volumes of seawater capable of meeting production requirements while complying with removal constraints for the targeted pathogenic bacterial strain.

Finally, based on our results, we proposed to predict the treatment capacities for different oyster farming applications. Because of the specific nature of the solar resource and the very high biosecured seawater requirements of oyster farming both in terms of volume and flow rate, photoreactors are not suitable for large-scale applications. However, this technological solution could be deployed for more specific uses that consume less water. The use of seawater for oyster hatcheries, or the development of pre-industrial installations, corresponding to daily volumes of the order of a few cubic meters, could be envisaged.

It is important to highlight that photocatalytic treatment can both degrade at the same time biotic and abiotic contaminant where to date hatcheries have to combine UVC disinfection to activated carbon column to achieve both biotic and abiotic pollutant elimination.

Availability of data

All the code used for the simulation of this publication are available on: https://github.com/CecileBlanchon/PhotocatalysisModelization.git

Acknowledgments

We would like to express our sincere gratitude to all the individuals and organizations that have contributed to the publication of this research paper. First, we would like to thank Pascal Romans and Nancy Trouillard, from the Oceanographic Observatory of Banyuls, for providing us the seawater used for all the experiments. Authors gratefully acknowledge Roger Garcia from PROMES for the drawings of the photoreactor. Finally, we would like to thank all the participants in this study for their time and willingness to share their experiences, thanks to Hervé Duval from PROMES, Marie-Agnès Travers from IHPE.

This work received support from the French National Research Agency (ANR) under grant number ANR-10-LABX-22-01-SOLSTICE, the Région Occitanie (PHOTODEPOL, N°19015248), and the University of Perpignan Via Domitia through the Energy Environment Research Federation (FREE) under projects “Lagoon Ecosystem Health and Remediation” and “PHOTOMIC” of the axis “Sustainable processes, management and ecosystem health”. This study is set within the framework of the “Laboratoire d’Excellence (LABEX)” TULIP (ANR-10-LABX-41). This work was also funded by the doctoral school Énergie - Environnement (ED305), University of Perpignan Via Domitia, France.

References

[1] B. Petton, D. Destoumieux-Garzón, F. Pernet, E. Toulza, J. de Lorgeril, L. Degremont, G. Mitta, The Pacific Oyster Mortality Syndrome, a Polymicrobial and Multifactorial Disease:

State of Knowledge and Future Directions, Front. Immunol. 12 (2021) 630343. https://doi.org/10.3389/fimmu.2021.630343.
[2] W.L. King, C. Jenkins, J.R. Seymour, M. Labbate, Oyster disease in a changing environment: Decrypting the link between pathogen, microbiome and environment, Mar. Environ. Res. 143 (2019) 124–140. https://doi.org/10.1016/j.marenvres.2018.11.007.
[3] J. Go, A. Deutscher, Z. Spiers, K. Dahle, P. Kirkland, C. Jenkins, Mass mortalities of unknown aetiology in Pacific oysters Crassostrea gigas in Port Stephens, New South Wales, Australia, Dis. Aquat. Organ. 125 (2017) 227–242. https://doi.org/10.3354/dao03146.
[4] D. Oyanedel, A. Lagorce, M. Bruto, P. Haffner, A. Morot, Y. Dorant, S. De La Forest Divonne, F. Delavat, N. Inguimbert, C. Montagnani, B. Morga, E. Toulza, C. Chaparro, J.-M. Escoubas, Y. Labreuche, Y. Gueguen, J. Vidal-Dupiol, J. De Lorgeril, B. Petton, L. Degremont, D. Tourbiez, L.-L. Pimparé, M. Leroy, O. Romatif, J. Pouzadoux, G. Mitta, F.L. Roux, G.M. Charrière, M.-A. Travers, D. Destoumieux-Garzón, Cooperation and cheating orchestrate *Vibrio* assemblages and polymicrobial synergy in oysters infected with OsHV-1 virus, (2023). https://doi.org/10.1101/2023.02.11.528104.
[5] H. Wang, B. Yang, X. Li, Q. Li, S. Liu, Screening of bacterial pathogens associated with mass summer mortality of the Pacific oyster, Crassostrea gigas, in China, Aquac. Rep. 20 (2021) 100672. https://doi.org/10.1016/j.aqrep.2021.100672.
[6] D. Saulnier, S. De Decker, P. Haffner, L. Cobret, M. Robert, C. Garcia, A Large-Scale Epidemiological Study to Identify Bacteria Pathogenic to Pacific Oyster Crassostrea gigas and Correlation Between Virulence and Metalloprotease-like Activity, Microb. Ecol. 59 (2010) 787–798. https://doi.org/10.1007/s00248-009-9620-y.
[7] A.L. Bourquet, C. Meneur, G. Oudot, P. Bodin, A. Granet, P. Blanchier, T. Renault, B. Morga, Mortalités d'huîtres creuse Crassostrea gigas : Étude du prégrossissement d'huîtres en marais salé en réponse aux mortalités, 2016. https://creaa.pagesperso-orange.fr/Doc%20actualite/RappPr%C3%A9goMaraisDef.pdf.
[8] Ifremer, Unité Expérimentale Mollusques Marins Atlantique, Les zones expérimentales de la Plateforme Molusque Marin de Bouin, EMMA (2022). https://emma.ifremer.fr/La-PMMB/Les-zones-experimentales/La-plateforme-securisee (accessed October 10, 2023).
[9] Ifremer, Présentation de la Plateforme expérimentale Mollusques Marins de La Tremblade, EMMA (2022). https://emma.ifremer.fr/La-PMMLT/Presentation (accessed October 10, 2023).
[10] M.M. Helm, N. Bourne, A. Lovatelli, N. Bourne, FAO, eds., Hatchery culture of bivalves: a practical manual, Food and Agriculture Organization of the United Nations, Rome, 2004.
[11] M. Miguet, V. Goetz, G. Plantard, Y. Jaeger, Removal of a Chlorinated Volatile Organic Compound (Perchloroethylene) from the Aqueous Phase by Adsorption on Activated Carbon, Ind. Eng. Chem. Res. 54 (2015) 9813–9823. https://doi.org/10.1021/acs.iecr.5b02364.
[12] T. Janin, Traitement d'effluents phytosanitaires par héliocatalyse – Hybridation sorption/photocatalyse, 2011.
[13] V. Yangali-Quintanilla, S.K. Maeng, T. Fujioka, M. Kennedy, G. Amy, Proposing nanofiltration as acceptable barrier for organic contaminants in water reuse, J. Membr. Sci. 362 (2010) 334–345. https://doi.org/10.1016/j.memsci.2010.06.058.
[14] C. Bellona, J. Drewes, Viability of a low-pressure nanofilter in treating recycled water for water reuse applications: A pilot-scale study, Water Res. 41 (2007) 3948–3958. https://doi.org/10.1016/j.watres.2007.05.027.

[15] V.C. Mota, H. Brenne, M. Kojen, K.R. Marhaug, M.E. Jakobsen, Evaluation of an ultrafiltration membrane for the removal of fish viruses and bacteria in aquaculture water, Front. Mar. Sci. 9 (2022) 1037017. https://doi.org/10.3389/fmars.2022.1037017.
[16] B. Zhou, J. Luo, M. Jin, N. Xue, R. He, W. Li, T. He, Micropollutants removal from aquaculture water using layer-by-layer self-assembled nanofiltration membranes, Water Res. (2024) 122933. https://doi.org/10.1016/j.watres.2024.122933.
[17] J. Mendret, A. Azais, T. Favier, S. Brosillon, Urban wastewater reuse using a coupling between nanofiltration and ozonation: Techno-economic assessment, Chem. Eng. Res. Des. 145 (2019) 19–28. https://doi.org/10.1016/j.cherd.2019.02.034.
[18] J.-M. Herrmann, Heterogeneous photocatalysis: state of the art and present applications In honor of Pr. R.L. Burwell Jr. (1912–2003), Former Head of Ipatieff Laboratories, Northwestern University, Evanston (Ill)., Top. Catal. 34 (2005) 49–65. https://doi.org/10.1007/s11244-005-3788-2.
[19] C. Minero, Kinetic analysis of photoinduced reactions at the water semiconductor interface, Catal. Today 54 (1999) 205–216. https://doi.org/10.1016/S0920-5861(99)00183-2.
[20] N. Serpone, Relative photonic efficiencies and quantum yields in heterogeneous photocatalysis, (1997).
[21] T. Janin, V. Goetz, S. Brosillon, G. Plantard, Solar photocatalytic mineralization of 2,4-dichlorophenol and mixtures of pesticides: Kinetic model of mineralization, Sol. Energy 87 (2013) 127–135. https://doi.org/10.1016/j.solener.2012.10.017.
[22] brice Reoyo-Prats, J.-C. Claire, H. Mouldi, G. Vincent, C.-B. Carole, P. Gaël, Photo-oxidation of three major pharmaceuticals in urban wastewater under artificial and solar irradiations, J. Photochem. Photobiol. Chem. 425 (2022) 113673. https://doi.org/10.1016/j.jphotochem.2021.113673.
[23] B. Reoyo-Prats, S. Anastasia, K. Somar, L.G.L. Corinne, W. Karine, G. Vincent, P. Gaël, Continuous degradation of micropollutants in real world treated wastewaters by photooxidation in dynamic conditions, Water Res. 221 (2022) 118777. https://doi.org/10.1016/j.watres.2022.118777.
[24] M. Kacem, G. Plantard, M. Brienza, V. Goetz, Continuous-Flow Aqueous System for Heterogeneous Photocatalytic Disinfection of Gram-Negative *Escherichia coli*, Ind. Eng. Chem. Res. 56 (2017) 15001–15007. https://doi.org/10.1021/acs.iecr.7b03644.
[25] M. Kacem, V. Goetz, G. Plantard, N. Wery, Modeling heterogeneous photocatalytic inactivation of *E . coli* using suspended and immobilized TiO_2 reactors, AIChE J. 61 (2015) 2532–2542. https://doi.org/10.1002/aic.14834.
[26] M. Kacem, G. Plantard, N. Wery, V. Goetz, Kinetics and efficiency displayed by supported and suspended TiO2 catalysts applied to the disinfection of Escherichia coli, Chin. J. Catal. 35 (2014) 1571–1577. https://doi.org/10.1016/S1872-2067(14)60212-6.
[27] M. Becker, M. Böhmer, Solar Thermal Concentrating Technologies, in: Vol 1 - 3 Proc. 8th Int. Symp. Sol. Therm. Conc. Technol. Köln Oct. 6 - 11 1996, C.F. Müller, Heidelberg, 1997. https://elib.dlr.de/31072/ (accessed October 20, 2023).
[28] J. Moreno-Andrés, M. Tierno-Galán, L. Romero-Martínez, A. Acevedo-Merino, E. Nebot, Inactivation of the waterborne marine pathogen Vibrio alginolyticus by photo-chemical processes driven by UV-A, UV-B, or UV-C LED combined with H2O2 or HSO5−, Water Res. 232 (2023) 119686. https://doi.org/10.1016/j.watres.2023.119686.
[29] H. Baniamerian, M. Safavi, M. Alvarado-Morales, P. Tsapekos, I. Angelidaki, S. Shokrollahzadeh, Photocatalytic inactivation of Vibrio fischeri using Fe2O3-TiO2-based

nanoparticles, Environ. Res. 166 (2018) 497–506.
https://doi.org/10.1016/j.envres.2018.06.011.
[30] F. Ren, Y. Li, M. Zhang, W. Chen, W. Chen, H. Chen, Photocatalytic inactivation mechanism of nano-BiPO4 against Vibrio parahaemolyticus and its application in abalone, Food Res. Int. 177 (2024) 113806. https://doi.org/10.1016/j.foodres.2023.113806.
[31] F. Correia, V. Goetz, G. Plantard, D. Sacco, A Model for Solar Photocatalytic Mineralization, J. Sol. Energy Eng. 133 (2011) 031002. https://doi.org/10.1115/1.4004242.
[32] S. Malato, P. Fernández-Ibáñez, M.I. Maldonado, J. Blanco, W. Gernjak, Decontamination and disinfection of water by solar photocatalysis: Recent overview and trends, Catal. Today 147 (2009) 1–59. https://doi.org/10.1016/j.cattod.2009.06.018.
[33] V. Goetz, C. Dezani, E. Ribeiro, C. Caliot, G. Plantard, Continuous flow photocatalytic reactor using TiO_2 -coated foams, modeling and experimental operating mode, AIChE J. 69 (2023) e17972. https://doi.org/10.1002/aic.17972.
[34] J. Blanco, S. Malato, P. Fernández-Ibañez, D. Alarcón, W. Gernjak, M.I. Maldonado, Review of feasible solar energy applications to water processes, Renew. Sustain. Energy Rev. 13 (2009) 1437–1445. https://doi.org/10.1016/j.rser.2008.08.016.
[35] S. Malato Rodríguez, J. Blanco Gálvez, M.I. Maldonado Rubio, P. Fernández Ibáñez, D. Alarcón Padilla, M. Collares Pereira, J. Farinha Mendes, J. Correia De Oliveira, Engineering of solar photocatalytic collectors, Sol. Energy 77 (2004) 513–524.
https://doi.org/10.1016/j.solener.2004.03.020.
[36] G. Plantard, C. Dezani, E. Ribeiro, B. Reoyo-Prats, V. Goetz, Modelling heterogeneous photocatalytic oxidation using suspended TiO_2 in a photoreactor working in continuous mode: Application to dynamic irradiation conditions simulating typical days in July and February, Can. J. Chem. Eng. 99 (2021) 142–152. https://doi.org/10.1002/cjce.23870.
[37] A.V. Emeline, V. Ryabchuk, N. Serpone, Factors affecting the efficiency of a photocatalyzed process in aqueous metal-oxide dispersions Prospect of distinguishing between two kinetic models, (2000) 9.
[38] G. Plantard, V. Goetz, Experimental and numerical studies of a solar photocatalytic process in a dynamic mode applied to three catalyst media, Chem. Eng. Process. Process Intensif. 62 (2012) 129–136. https://doi.org/10.1016/j.cep.2012.08.002.
[39] V. Goetz, T. Janin, G. Plantard, S. Brosillon, Hybridation between Heterogeneous Photocatalysis and Adsorption, Int. J. Eng. Pract. Res. 2 (2013).
[40] P.S.M. Dunlop, C.P. Sheeran, J.A. Byrne, M.A.S. McMahon, M.A. Boyle, K.G. McGuigan, Inactivation of clinically relevant pathogens by photocatalytic coatings, J. Photochem. Photobiol. Chem. 216 (2010) 303–310.
https://doi.org/10.1016/j.jphotochem.2010.07.004.
[41] S. Kim, K. Ghafoor, J. Lee, M. Feng, J. Hong, D.-U. Lee, J. Park, Bacterial inactivation in water, DNA strand breaking, and membrane damage induced by ultraviolet-assisted titanium dioxide photocatalysis, Water Res. 47 (2013) 4403–4411.
https://doi.org/10.1016/j.watres.2013.05.009.
[42] C. Blanchon, E. Toulza, C. Calvayrac, G. Plantard, Heterogeneous photo-oxidation in microbial inactivation :A promising technology for seawater bio-securing?, (2023).
[43] H. Chick, An Investigation of the Laws of Disinfection, J. Hyg. (Lond.) 8 (1908) 92–158. https://doi.org/10.1017/S0022172400006987.
[44] O.K. Dalrymple, E. Stefanakos, M.A. Trotz, D.Y. Goswami, A review of the mechanisms and modeling of photocatalytic disinfection, (2010) 12.

[45] O.K. Dalrymple, D.Y. Goswami, Mechanistic Modeling of Photocatalytic Water Disinfection, in: T. An, H. Zhao, P.K. Wong (Eds.), Adv. Photocatalytic Disinfect., Springer Berlin Heidelberg, Berlin, Heidelberg, 2011: pp. 273–315. https://doi.org/10.1007/978-3-662-53496-0_13.
[46] P. Ganguly, C. Byrne, A. Breen, S.C. Pillai, Antimicrobial activity of photocatalysts: Fundamentals, mechanisms, kinetics and recent advances, Appl. Catal. B Environ. 225 (2018) 51–75. https://doi.org/10.1016/j.apcatb.2017.11.018.
[47] L.W. Hom, Kinetics of chlorine disinfection in an ecosystem, (1972). https://ascelibrary.org/doi/pdf/10.1061/JSEDAI.0001370.
[48] R.J.W. Lambert, M.D. Johnston, Disinfection kinetics: a new hypothesis and model for the tailing of log-survivor/time curves, J. Appl. Microbiol. 88 (2000) 907–913. https://doi.org/10.1046/j.1365-2672.2000.01060.x.
[49] H.E. Watson, A Note on the Variation of the Rate of Disinfection with Change in the Concentration of the Disinfectant, Epidemiol. Infect. 8 (1908) 536–542. https://doi.org/10.1017/S0022172400015928.
[50] M. Otaki, T. Hirata, S. Ohgaki, Aqueous microorganisms inactivation by photocatalytic reaction, Water Sci. Technol. 42 (2000) 103–108. https://doi.org/10.2166/wst.2000.0365.
[51] C. Sichel, J. Tello, M. de Cara, P. Fernández-Ibáñez, Effect of UV solar intensity and dose on the photocatalytic disinfection of bacteria and fungi, Catal. Today 129 (2007) 152–160. https://doi.org/10.1016/j.cattod.2007.06.061.
[52] C. McCullagh, J.M.C. Robertson, D.W. Bahnemann, P.K.J. Robertson, The application of TiO2 photocatalysis for disinfection of water contaminated with pathogenic micro-organisms: a review, Res. Chem. Intermed. 33 (2007) 359–375. https://doi.org/10.1163/156856707779238775.
[53] D. Gumy, C. Morais, P. Bowen, C. Pulgarin, S. Giraldo, R. Hajdu, J. Kiwi, Catalytic activity of commercial of TiO2 powders for the abatement of the bacteria (E. coli) under solar simulated light: Influence of the isoelectric point, Appl. Catal. B Environ. 63 (2006) 76–84. https://doi.org/10.1016/j.apcatb.2005.09.013.
[54] F. Correia, Etude expérimentale et modélisation de réacteurs photochimiques solaires : Performances de médias photocatalytiques, 2011.
[55] M. Kacem, Inactivation bactérienne par photocatalyse hétérogène Application à Escherichia coli, 2015.
[56] C. Dezani, Photo catalyse hétérogène en réacteurs ouverts pour la gestion de la ressource solaire : expérimentations sur différents médias et modélisations, 2021.
[57] C. Dezani, E. Ribeiro, V. Goetz, G. Plantard, Continuous flow photoreactor undergoing variable simulated irradiation conditions: Experimentations and modeling, Chem. Eng. J. Adv. 12 (2022) 100422. https://doi.org/10.1016/j.ceja.2022.100422.
[58] Solomit OASU, Visualisation des données | Somlit, solomit.fr (2018). https://www.somlit.fr/visualisation-des-donnees/ (accessed December 18, 2024).
[59] A. Cibrario, Diversité génétique et phénotypique de l'espèce Brettanomyces bruxellensis: influence sur son potentiel d'altération des vins rouges, 2019.
[60] A.H. Geeraerd, C.H. Herremans, J.F. Van Impe, Structural model requirements to describe microbial inactivation during a mild heat treatment, Int. J. Food Microbiol. 59 (2000) 185–209. https://doi.org/10.1016/S0168-1605(00)00362-7.
[61] M.D. Labas, C.A. Martín, A.E. Cassano, Kinetics of bacteria disinfection with UV radiation in an absorbing and nutritious medium, Chem. Eng. J. 114 (2005) 87–97. https://doi.org/10.1016/j.cej.2005.09.013.

[62] J. Marugán, R. van Grieken, C. Sordo, C. Cruz, Kinetics of the photocatalytic disinfection of Escherichia coli suspensions, Appl. Catal. B Environ. 82 (2008) 27–36. https://doi.org/10.1016/j.apcatb.2008.01.002.
[63] B.F. Severin, M.T. Suidan, R.S. Engelbrecht, Kinetic modeling of U.V. disinfection of water, Water Res. 17 (1983) 1669–1678. https://doi.org/10.1016/0043-1354(83)90027-1.
[64] D. Rubio, E. Nebot, J.F. Casanueva, C. Pulgarin, Comparative effect of simulated solar light, UV, UV/H2O2 and photo-Fenton treatment (UV–Vis/H2O2/Fe2+,3+) in the Escherichia coli inactivation in artificial seawater, Water Res. 47 (2013) 6367–6379. https://doi.org/10.1016/j.watres.2013.08.006.
[65] J. Marugán, R. van Grieken, A.E. Cassano, O.M. Alfano, Kinetic modelling of the photocatalytic inactivation of bacteria, Water Sci. Technol. 61 (2010) 1547–1553. https://doi.org/10.2166/wst.2010.057.
[66] C. Blanchon, E. Toulza, C. Calvayrac, S. Eichendorff, M.-A. Travers, J. Vidal-Dupiol, C. Montagnani, J.-M. Escoubas, C. Stavrakakis, G. Plantard, Inactivation of two oyster pathogens by photocatalysis and monitoring of changes in the microbiota of seawater: A case study on Ostreid herpes virus 1 µVar and Vibrio harveyi., Chemosphere 346 (2024) 140565. https://doi.org/10.1016/j.chemosphere.2023.140565.
[67] S. Malato, J. Cáceres, A.R. Fernández-Alba, L. Piedra, M.D. Hernando, A. Agüera, J. Vial, Photocatalytic Treatment of Diuron by Solar Photocatalysis: Evaluation of Main Intermediates and Toxicity, Environ. Sci. Technol. 37 (2003) 2516–2524. https://doi.org/10.1021/es0261170.
[68] S. Malato, J. Blanco, A. Vidal, C. Richter, Photocatalysis with solar energy at a pilot-plant scale: an overview, Appl. Catal. B Environ. 37 (2002) 1–15. https://doi.org/10.1016/S0926-3373(01)00315-0.
[69] A.P. Schuch, N.C. Moreno, N.J. Schuch, C.F.M. Menck, C.C.M. Garcia, Sunlight damage to cellular DNA: Focus on oxidatively generated lesions, Free Radic. Biol. Med. 107 (2017) 110–124. https://doi.org/10.1016/j.freeradbiomed.2017.01.029.
[70] J.C. Lagarias, J.A. Reeds, M.H. Wright, P.E. Wright, Convergence Properties of the Nelder--Mead Simplex Method in Low Dimensions, SIAM J. Optim. 9 (1998) 112–147. https://doi.org/10.1137/S1052623496303470.
[71] L. Megatif, R. Dillert, D.W. Bahnemann, Determination of the quantum yield of a heterogeneous photocatalytic reaction employing a black body photoreactor, Catal. Today 355 (2020) 698–703. https://doi.org/10.1016/j.cattod.2019.06.008.
[72] E. Ribeiro, G. Plantard, V. Goetz, TiO2 grafted activated carbon elaboration by milling: Composition effect on sorption and photocatalytic properties, J. Photochem. Photobiol. Chem. 408 (2021) 113108. https://doi.org/10.1016/j.jphotochem.2020.113108.
[73] E. Ribeiro, Composites Charbon-Actif/TiO2 pour des applications solaires, 2020.
[74] E.D. Silva, Développement d'outils analytiques innovants pour le suivi des populations de Vibrio dans les environnements aquatiques, 2017.
[75] France Naissain, Prégrossissement (T8 à 55 unités/kg.), (2023). https://www.francenaissain.com/nos-produits/pregrossissement-t8-a-55-unites-kg/ (accessed October 18, 2023).
[76] G. Plantard, B. Reoyo-Prats, A. Sellier, S. Khaska, C. Le Gall Lasalle, K. Weiss, V. Goetz, Performances of a pool-type photoreactor operating in continuous mode under solar irradiation for the treatment of pollutants contained in wastewater, Chem. Eng. Sci. (2023).

Figures :

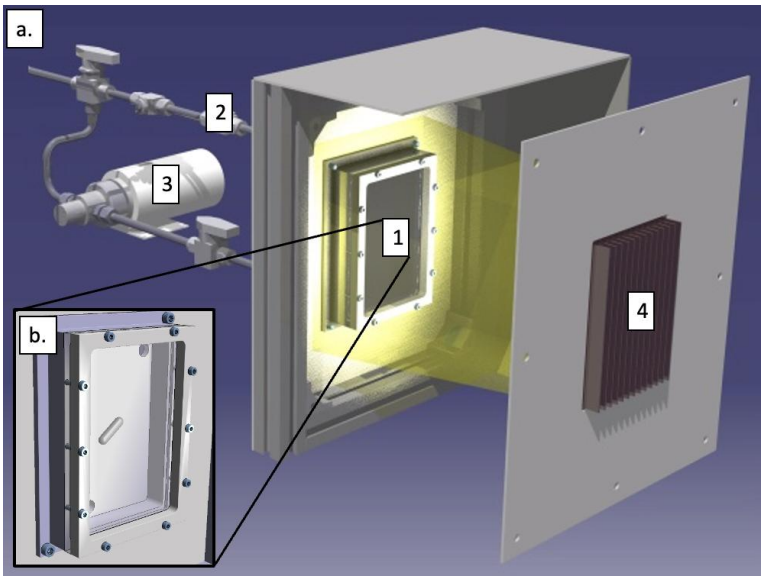

Figure 1: Presentation of the apparatus (drawing from Roger Garcia, PROMES): pilot (a) composed of the photoreactor (1), the recirculating loop (2) with the centrifugal pump (3) and the UV LED panel (4). The figure (b) shows a closed view of the photoreactor.

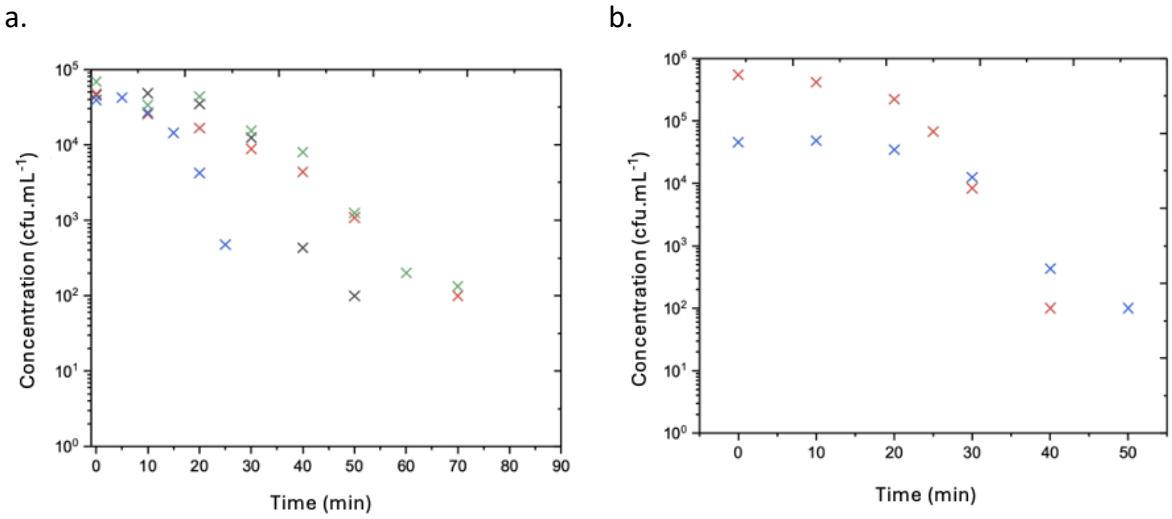

Figure 2: Photocatalysis of Vibrio harveyi in batch (a) at different flux density (10 W.m^{-2} (x), 20 W.m^{-2} (x), 35 W.m^{-2} (x), and 45 W.m^{-2} (x)), and (b) at different bacterial concentrations (at 35 W.m^{-2}). Experiments were performed in natural seawater (pH 8 et salinity of 35 PSU) with titanium dioxide concentration of 4 g.L^{-1}. Each experimental point was the average of three experiments with a variation coefficient lower than 35%.

Table 1: optimal constants found from batch experiments

	α ($s^{f-1}.J^{-f}.cfu^{1-n}$)	n	f	β ($L.cfu^{-1}$)	β' ($m^2.W^{-1}$)	MRE (%)
Model N°1 $\dot{r} = \alpha.(S.I_{(t)})^f.C.V_r$	0.003	Fixed at 1	0.337	Fixed at 0	Fixed at 0	6.0
Model N°2	0.004	Fixed at 1	0.338	Fixed at 0	$1.4x10^{-16}$	6.0

$\dot{r} = \alpha.(S.I_{(t)})^f.\frac{C.V_r}{\beta'.C.V_r+1}$						
Model N°3 $\dot{r} = \alpha.(S.I_{(t)})^f.(C.V_r)^n$	**0.0007**	**1.13**	**0.311**	Fixed at 0	Fixed at 0	**5.6**
Model N°4 $\dot{r} = \alpha.(C.V_r)^n.\frac{S.I_{(t)}}{\beta.S.I_{(t)}+1}$	0.002	1.21	Fixed at 1	5.67	Fixed at 0	5.7
Model N°5 $\dot{r} = \alpha.\frac{S.I_{(t)}}{\beta.S.I_{(t)}+1}.\frac{C.V_r}{\beta'.C.V_r+1}$	0.03	Fixed at 1	Fixed at 1	7.17	$4.8x.10^{-17}$	6.1

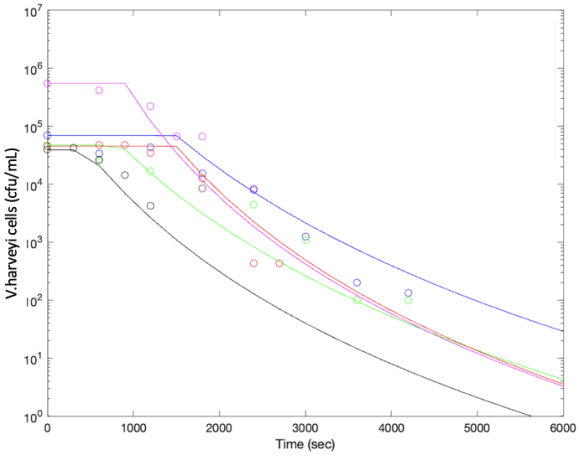

Figure 3: Kinetic inactivation curves obtained for the determination of the best fitting kinetic law : model N°3, (—) for I = 10 W.m^{-2} and C_0 = 10^5 cfu.mL^{-1}, (—) for I = 20 W.m^{-2} and C_0 = 10^5 cfu.mL^{-1}, (—) for I = 35 W.m^{-2} and C_0 = 10^5 cfu.mL^{-1}, (—) for I = 45 W.m^{-2} and C_0 = 10^5 cfu.mL^{-1}, and (—) for I = 35 W.m^{-2} and C_0 = 10^6 cfu.mL^{-1},

a.

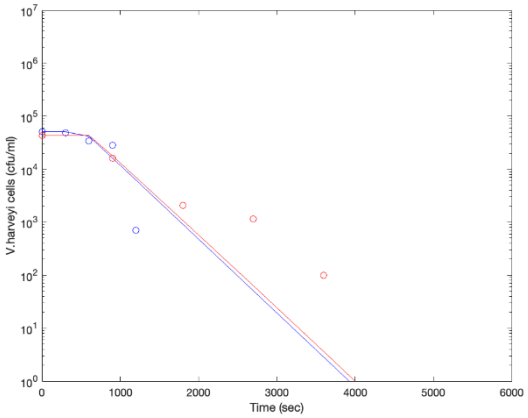

b.

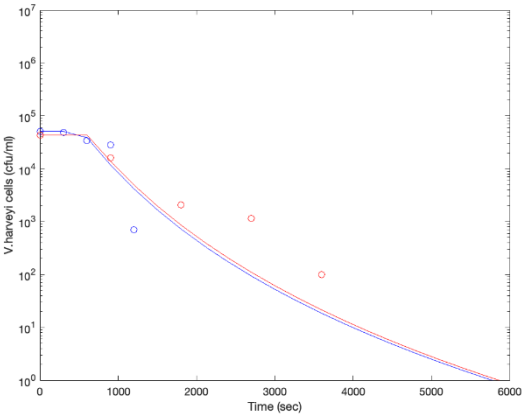

c.

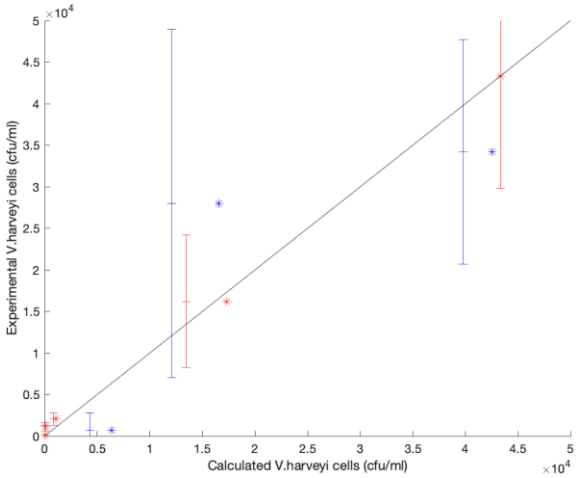

Figure 4: Kinetic inactivation curves obtained for independent experimental data (a) model N°1 (MRE = 4% and 11% respectively for the experimental data N°1 and N°2), (b) model N°3 (MRE = 4% and 8% respectively for the experimental data N°1 and N°2), and (c) the diagram of dispersion for the comparison of the experimental results (two experiments at I = 45 W.m-2, with an initial concentration of 5x10^3 cfu.mL^{-1} in blue and 4x10^4 cfu.mL^{-1} in red) and the calculated results obtained for the model N°1 (*), the model N°3 (+).

Table 2: solar characteristics for each month at each French place (based on Meteonorm data)

	January	February	March	Avril	May	Jun	July	August	September	October	November	December	Total year
	Average day												
	Cumulative energy received (kJ.m^{-2})												
Montpellier	305	480	713	907	1 099	1 273	1 275	1 049	821	508	347	266	275 512
Bordeaux	240	383	607	802	974	1 097	1 066	942	732	468	271	197	237 304
Nantes	189	339	546	788	957	1 083	1 038	917	716	401	234	162	224 641
Day duration (h)	8	9	12	13	15	15	15	14	13	11	9	8	/

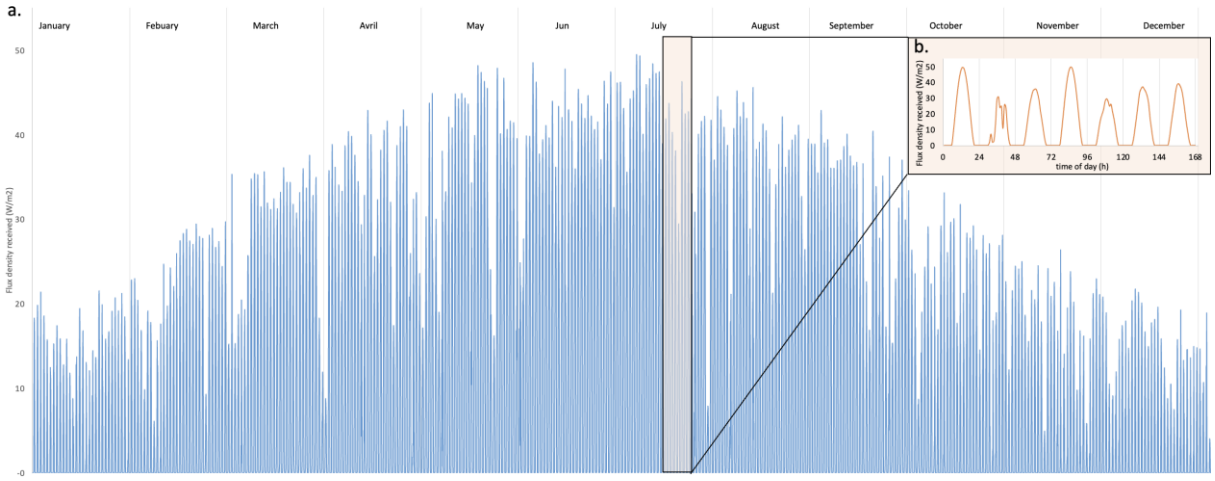

c.

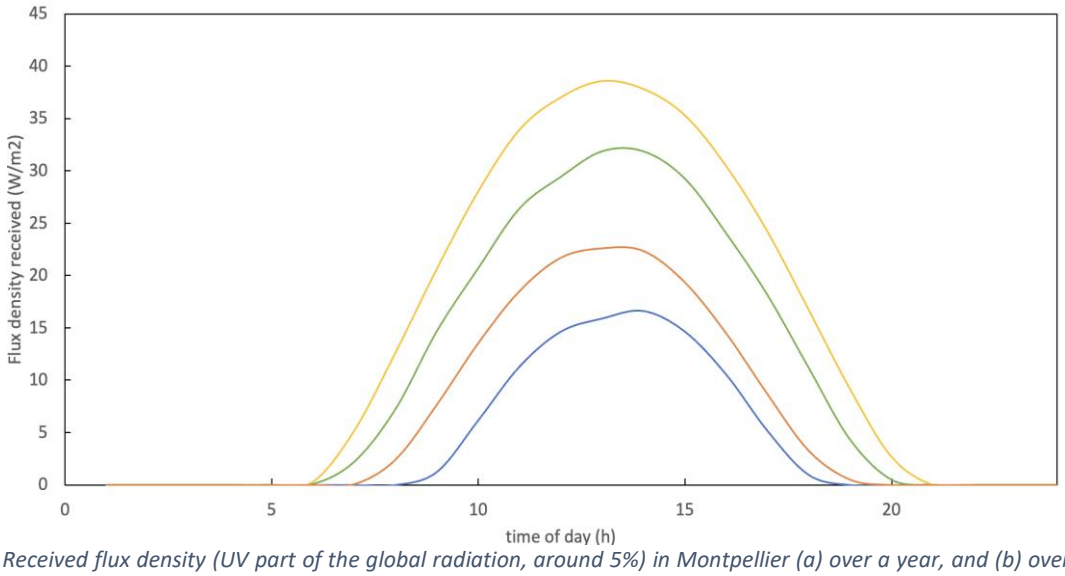

Figure 5: Received flux density (UV part of the global radiation, around 5%) in Montpellier (a) over a year, and (b) over a week in July, and (c) for average day of each season: — Summer, — Spring, — Autumn, and — Winter,.

a.

b.

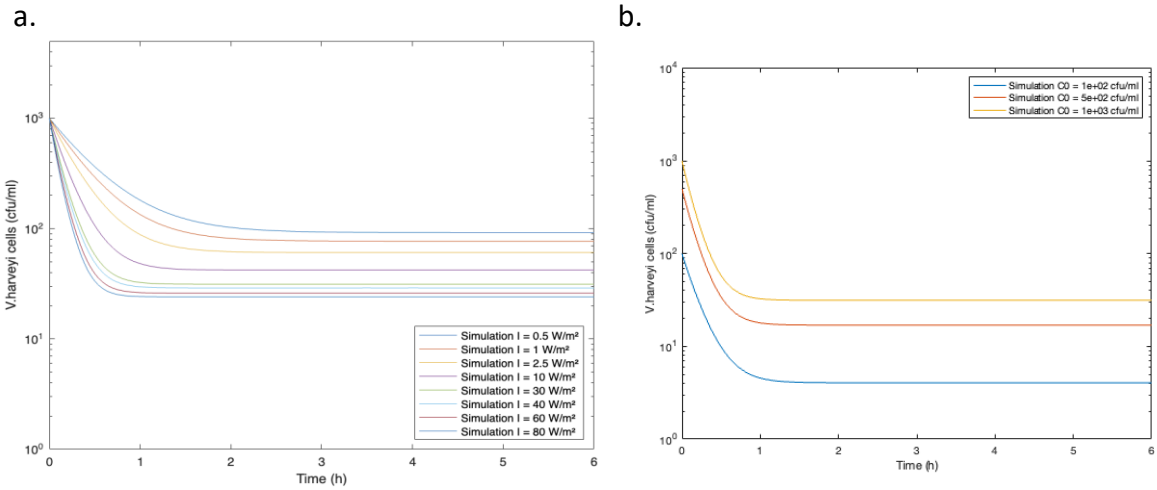

c.

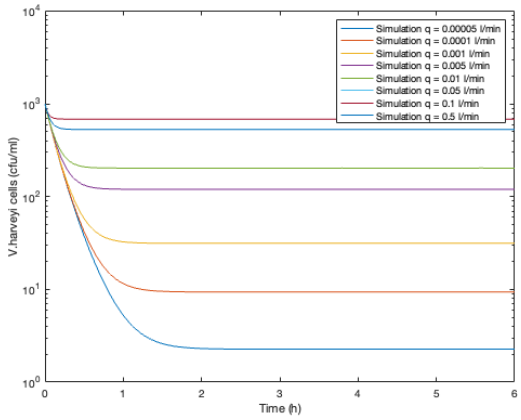

Figure 6: individual influence of each operating parameter on bacterial inactivation by open mode photocatalysis: (a) different flux density I with $C_0 = 10^3$ cfu.ml^{-1} and q = 1 mL.min^{-1}, (b) different bacterial feed concentrations C_0 with I = 30 W.m^{-2} and q = 1 mL.min^{-1}, and (c) different flow rates q with $C_0 = 10^3$ cfu.ml^{-1} and I = 30 W.m^{-2}.

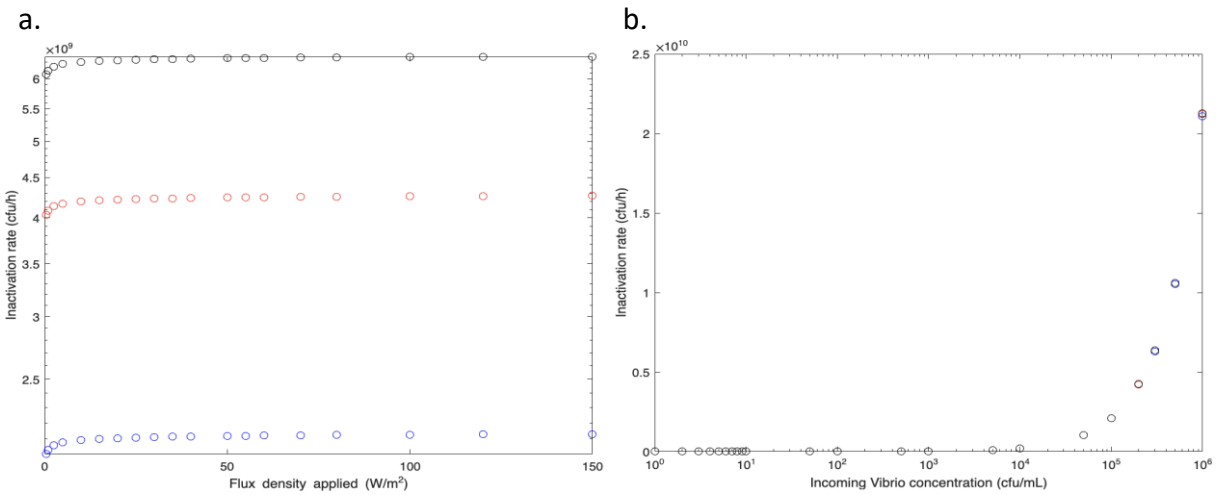

Figure 7: Inactivation rate once the equilibrium of the reactor was reached depending (a) on the flux density applied (with a feed solution of bacteria of 10^5 cfu.mL^{-1} (o), 2x10^5 cfu.mL^{-1} (o), and 3x10^5 cfu.mL^{-1} (o)), and (b) on the feed solution concentration (with a constant irradiation at 10 W.m^{-2} (o), 30 W.m^{-2} (o), and 45 W.m^{-2} (o)). (simulations performed with a constant flow rate q = 1 mL.min^{-1} using the same photoreactor dimension of that one used in batch).

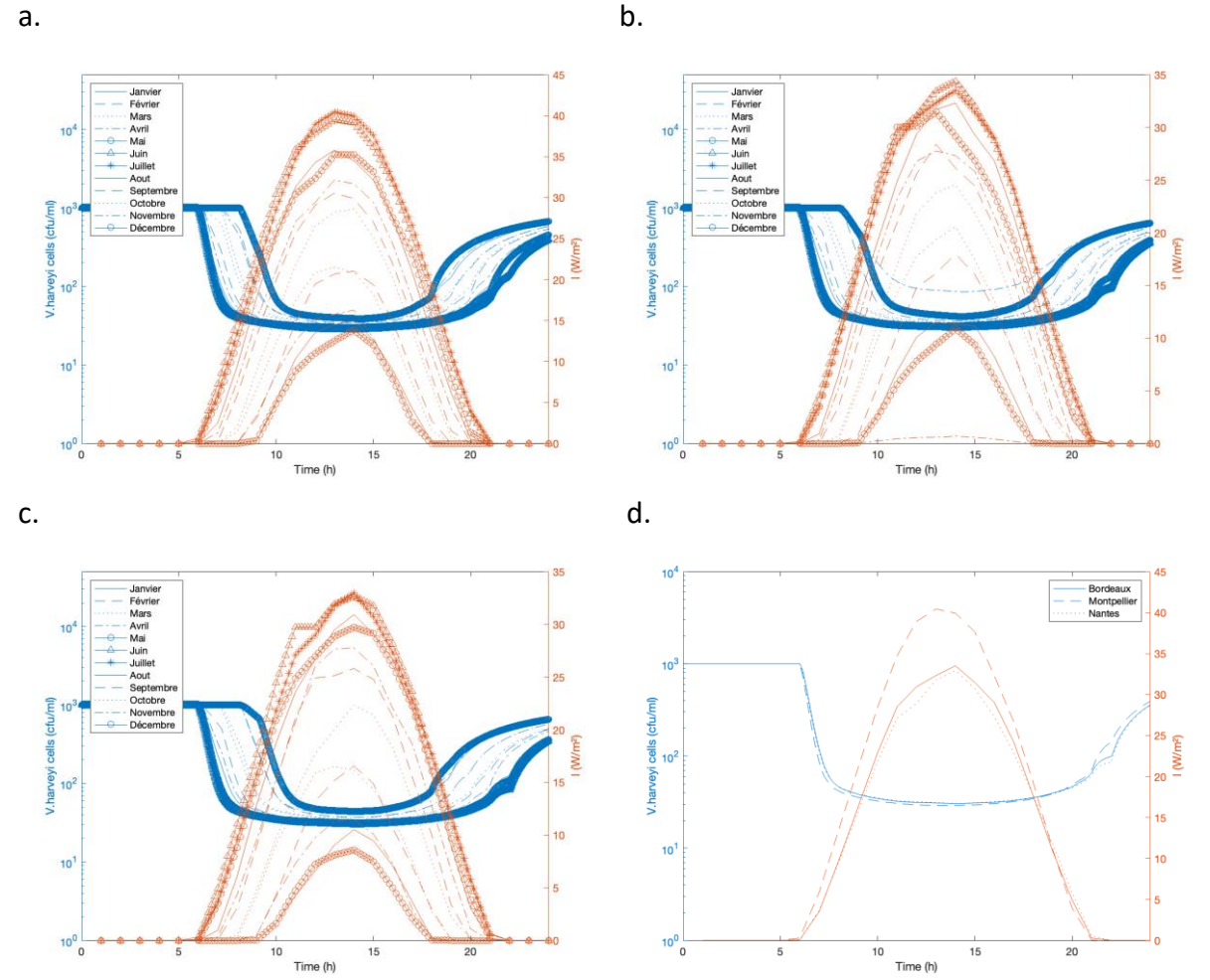

e.

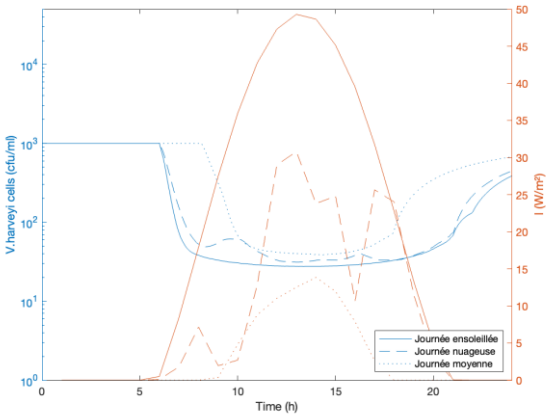

Figure 8: Daily Vibrio harveyi inactivation by photocatalysis for average day of each month in three locations close to aquaculture facilities (simulation performed with a constant flow rate q = 1 mL.min^{-1} and an feed solution at 10^3 cfu.mL^{-1} of Vibrio harveyi bacteria using the same photoreactor dimension of that one used in batch) (a) in Montpellier (France), (b) in Bordeaux (France), (c) in Nantes (France), (d) comparison of the three locations for the average day of July, and (e) comparison of daily irradiation in July at Montpellier.

Table 3: flow rate modulation effect on reactor performance, with cloudy day corresponding to day 2 of Fig. 9, sunny day to day 1 and average day to day 3.

		Constant flow rate (1 mL.min^{-1})			Modulated flow rate		
	Unit	Cloudy day	Sunny day	Average day	Cloudy day	Sunny day	Average day
Cumulative energy received	kJ	756	1 568	1 123	756	1 568	1 123
Average inactivation rate	cfu.h^{-1}	4 610	4 124	4 651	737	928	870
Volume of outlet at 99% inactivation	mL	0	0	0	152.4	199.8	185.2

a.

b.

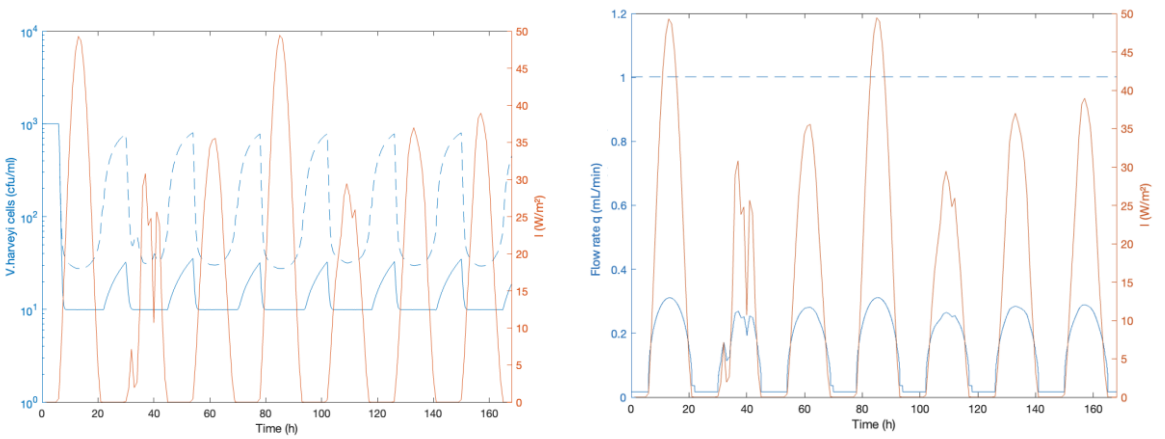

Figure 9: Bacteria inactivation depending of the applied flow rate (a) Vibrio harveyi concentration in outlet of the photoreactor depending on the flux density received on 7 days in July at Montpellier with an income pathogen concentration of 10^3 cfu.mL^{-1}, and (b) the applied flow rate. (—) with constant flow rate q=1 mL.min^{-1}, or (- -) with variable flow rate determined to inactivate 99% of income pathogens

Table 4: average daily treatable volume per square meter of photoreactor

	Irradiated surface S (m^2)	Photoreactor volume (L)	January	February	March	Avril	May	Jun	July	August	September	October	December
			Volume treated by day (L/day)										
Montpellier	1	19.7	38.9	50.2	61.8	72.0	81.1	87.2	86.5	77.4	66.8	52.7	34.7
Bordeaux	1	19.7	35.7	46.1	59.0	69.5	79.0	83.8	82.2	75.5	65. 1	51.5	34. 8
Nantes	1	19.7	32.4	43.9	57.1	69.5	79.4	84.2	82.4	75.6	64. 8	49.2	32.6

1